First-principles study of magnetoelastic effect in the difluoride compounds MF_2 (M = Mn, Fe, Co, Ni)

Hena Das,[1] Sudipta Kanungo,[2] and T. Saha-Dasgupta[2]
[1]*School of Applied and Engineering Physics, Cornell University, Ithaca, New York, USA*
[2]*S. N. Bose National Centre for Basic Sciences, Kolkata IN-700 098, India*
(Received 19 June 2012; revised manuscript received 31 July 2012; published 15 August 2012; corrected 21 February 2013)

Employing first-principles density-functional-theory-based calculations, we study the electronic structure and magnetoelastic effect in difluoride compounds MF_2 (M = Mn, Fe, Co, Ni). The magnetoelastic-effect-driven cell-parameter changes across the series are found to exhibit nonmonotonic behavior in agreement with recent experimental reports. Our study reveals that this originates from the nonmonotonicity in the exchange striction of the bond-stretching phonon mode associated with the short M-F bond. Our study also uncovers the role of M-F covalency in driving the nonmonotonic behavior of the M-M exchange interaction across the series.

DOI: 10.1103/PhysRevB.86.054422 PACS number(s): 75.80.+q, 71.15.Mb, 63.20.−e

I. INTRODUCTION

The interplay of spin, orbital, and lattice degrees of freedom in transition-metal oxides (TMOs) has been a lively field of study. The general interest in the response of lattices following changes in magnetism has been revived upon the surge of activity in the field of multiferroics and magnetoelastic effects. While attention has been focused primarily on oxide materials, much less attention has been given to the transition-metal fluorides (TMFs) with F^- ions in the system as opposed to O^{2-} ions. Exploring the fluorides may be a worthwhile exercise for the prediction of new multiferroic and magnetoelastic materials. There have already been theoretical predictions of ferroelectricity in perovskite-structured alkaline-earth metal fluorides like $NaCaF_3$ and $NaCdF_3$.[1] Based on the symmetry analysis, compounds like $KCrF_4$, $CsCoF_4$, and $KMnFeF_6$ have been predicted[2] to show linear magnetoelectric coupling even with the possibility of multiferroic behavior. One of the important mechanisms which can drive magnetoelectric behavior is that of magnetostriction, driven by the $\sum_{ij} J_{ij}\vec{S}_i\vec{S}_j$ term in the Hamiltonian. The simplest possible manifestation of the magnetostriction or the static magnetoelastic effect is the change in crystal dimensions, responding to the change in magnetism.

Recent neutron-powder-diffraction experiments[3,4] carried out on a series of transition-metal-difluoride compounds were reported to exhibit interesting magnetostriction effects at the magnetic transition. The compounds investigated include CrF_2, MnF_2, FeF_2, CoF_2, NiF_2, and CuF_2.[3,4] Interestingly, the involved transition metals (TMs) in the series are 3d TMs with increasing d occupation of d^4 to d^9. Among this series of compounds, CrF_2 and CuF_2 are structurally different, belonging to the distorted monoclinic space group rather than having the tetragonal structure adopted by the rest.[5] The ordered magnetic structures are also complicated[6] compared to MnF_2, FeF_2, CoF_2, and NiF_2 for which a nearly collinear A-type antiferromagnetic (A-AFM) structure is formed below the magnetic-ordering temperatures.[7] Leaving aside CrF_2 and CuF_2 and considering the high-spin state of M cations as expected for 3d TMFs, the magnetic moment should monotonically decrease from $S = \frac{5}{2}$ for MnF_2 to $S = 2$ for FeF_2 to $S = \frac{3}{2}$ for CoF_2 and $S = 1$ for NiF_2.

The measured magnetovolume effect, however, exhibits a rather nonmonotonic trend as a function of magnetic moment with a large negative value for MnF_2, moderately negative values for FeF_2 and NiF_2, and a positive value for CoF_2 (see Fig. 13 in Ref. 6). Although speculations have been made for this curious behavior, to the best of our knowledge, no first-principles investigation has been carried out except for the calculation of the phonon spectrum for MnF_2 (Ref. 8) and the investigation of the covalency effect in FeF_2 and NiF_2.[9] In the present study, we carry out a detailed and concise first-principles study of MnF_2, FeF_2, CoF_2, and NiF_2, helping us in uncovering the origin of this interesting behavior. The present study also establishes the applicability of the first-principles method in capturing even the tiny magnetoelastic effect correctly as in the present case.

II. METHODOLOGY

The density-functional-theory (DFT) calculations, reported in the present study, were carried out with a choice of three different basis sets: (a) the plane-wave-basis-based pseudopotential framework as implemented in the Vienna *Ab initio* Simulation package (VASP),[10] (b) the linear-muffin-tin-orbital (LMTO) basis[11] and its Nth-order extension (NMTO) basis[12] as implemented in the Stuttgart code,[13] and (c) the linear-augmented-plane-wave (LAPW) basis as implemented in WIEN2K code.[14] The consistency of results in three different basis sets has been cross-checked. The exchange-correlation function was chosen to be that of the generalized gradient approximation (GGA) implemented following the Perdew-Burke-Ernzerhof (PBE) prescription.[15] For the structural optimization, the positions of the ions were relaxed towards equilibrium until the Hellman-Feynman forces became less than 0.001 eV/Å. For the plane-wave calculation, a 600-eV plane-wave cutoff was used. A k-point mesh of $6 \times 6 \times 8$ in the Brillouin zone was used for self-consistent calculations. We have also carried out calculations in the presence of spin-orbit coupling (SOC) to know its importance in this series of compounds, also providing us with the information of magnetic anisotropic energy. SOC has been included in the calculation in scalar relativistic form as a perturbation to the original Hamiltonian.

III. CRYSTAL AND MAGNETIC STRUCTURE

Transition-metal difluorides, MF_2 (M = Mn, Fe, Co, Ni), crystallize in a tetragonal, rutile-type structure of the

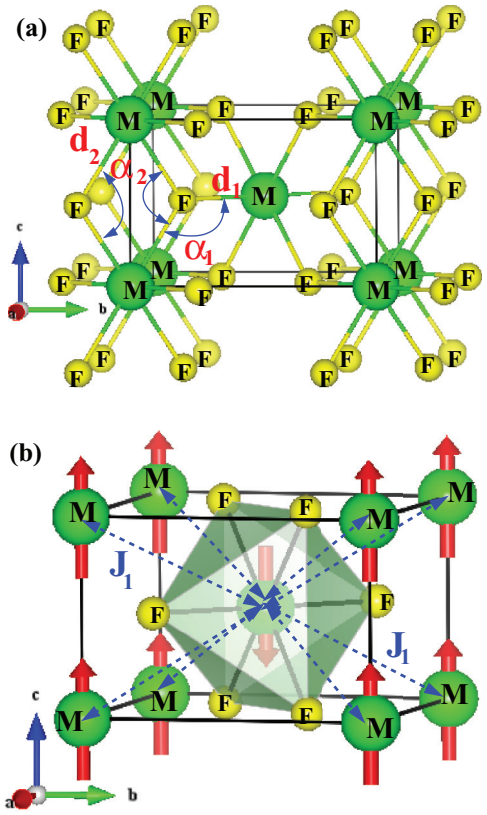

FIG. 1. (Color online) (a) Crystal and (b) magnetic structures of MF_2. The various important bond lengths and bond angles (see text for details) have been marked in the plot of the crystal structure while the nearest-neighbor magnetic interaction J_1 has been marked in the plot of the magnetic structure.

$P4_2/mnm$ space group as shown in Fig. 1(a). The small orthorhombic distortion of NiF_2 below the magnetic transition[9] has been neglected in our study as in the experimental analysis reported in Refs. 1 and 3. The M atoms occupy the high-symmetry Wyckoff position of $2a$ while the F atoms occupy the $4f$ Wyckoff positions with an associated free parameter x. The arrangement of the F^- ions surrounding the M^{2+} site is that of a distorted octahedra in term of four long and two short M-F bond lengths and F-M-F bond angles deviating from 90°. The tetragonal unit cell consists of two formula units with two M atoms in the unit cell, one at the corner of the cell and the other at the body-diagonal position. While two corner MF_6 octahedra are edge sharing along the crystallographic c direction, through the sharing of two F atoms, the MF_6 octahedra at the corner and body-diagonal positions are corner shared through the sharing of one F atom. The antiferromagnetic structure given by the propagation vector $\vec{k} = (0,0,1)$ involves antiparallel alignment of the corner M spins and that at the body-centered position as shown in Fig. 1(b). The corner-shared M-M antiferromagnetic coupling proceeds through one short M-F bond (d_1), one long M-F bond (d_2), and one M-F-M angle of ≈130°. The edge-shared M-M interaction which is of ferromagnetic nature in the A-type AFM structure proceeds through equal-sized long M-F bonds and M-F-M angles of ≈100°.

IV. ELECTRONIC STRUCTURE

Figure 2 shows the spin-polarized density of states (DOS) of MF_2 calculated within the GGA and projected onto M d and F p characters. The distortion of the MF_6 octahedra lifts the degeneracy of the M d levels completely in each of the compounds. The crystal-field splitting of metal d levels together with their occupancies are also shown in Fig. 2. The crystal-field splittings were calculated using the NMTO-downfolding method[12] in which M d states were kept active and the other degrees of freedom were downfolded or integrated out. This leads to the construction of an effective, low-energy M-d-only Hamiltonian. The on-site block of the real-space representation of this low-energy Hamiltonian provides the crystal-field splittings. For MnF_2, the majority d levels are completely filled, and the minority d levels are completely empty, giving rise to an insulating solution with a large band gap of above 2 eV and a total magnetic moment of $5\mu_B$/f.u. For FeF_2 and CoF_2, on the other hand, d^6 and d^7 occupations of Fe^{2+} and Co^{2+} ions, respectively, give rise to a partially filled t_{2g} manifold. Nevertheless, the finite splitting between the levels of the t_{2g} manifold on the order

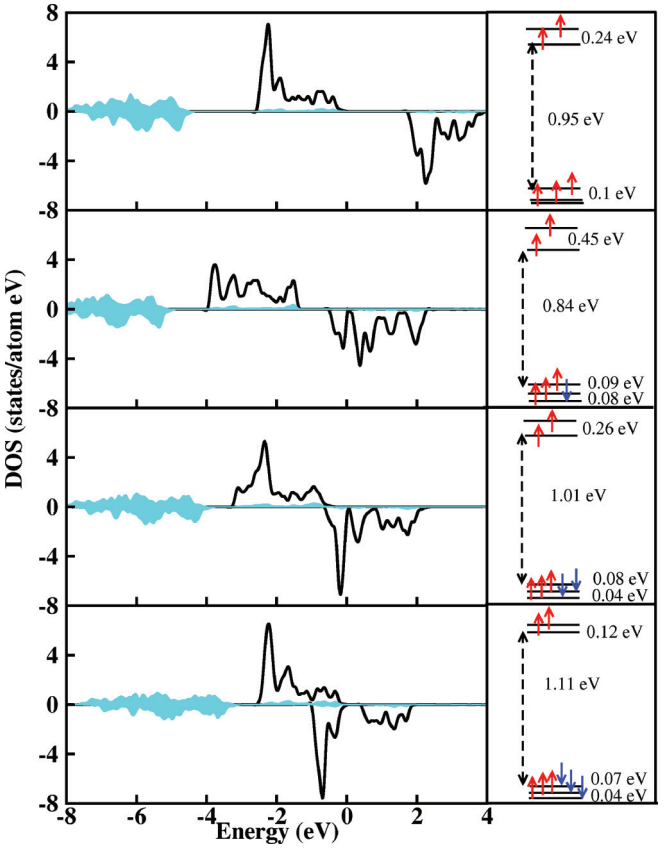

FIG. 2. (Color online) The left panels show the spin-polarized DOSs of MF_2 for M = Mn, Fe, Co, and Ni (from top to bottom, respectively). The solid, black line and shaded, cyan (gray) area represent the DOSs projected onto the M d and Fe p states, respectively. The zero of the energy is set at the GGA Fermi energy. The right panels show the crystal-field splitting as well as the occupancies of the M d levels for MF_2 for M = Mn, Fe, Co, and Ni (from top to bottom, respectively). The lowest two t_{2g} levels for Mn are almost degenerate with a tiny separation between them.

of 0.08–0.09 eV gives rise to an insulating solution with tiny band gaps even within GGA calculations. The total magnetic moments are obtained as integer values, $4\mu_B$/f.u. and $3\mu_B$/f.u. for FeF_2 and CoF_2, respectively, in conformity with the insulating solutions. For NiF_2, the large crystal-field splitting between the t_{2g} and e_g manifolds give rise to a moderate gap value of 1 eV with a total magnetic moment of $2\mu_B$/f.u. and d^8 nominal occupancy of Ni^{2+}. We notice that the F-p-dominated DOS is separated from the M-d-dominated DOS by a gap, the size of which decreases moving from MnF_2 to FeF_2 to CoF_2 to NiF_2 and which in turn increases in the relative hybridization between the M d and F p degrees of freedom. This is reflected in the computed magnetic moment residing at the F site, which turns out to be $0.10\mu_B$, $0.12\mu_B$, $0.13\mu_B$, and $0.15\mu_B$ for MnF_2, FeF_2, CoF_2, and NiF_2, respectively. We also carried out GGA + SOC calculations, considering the spin-quantization axis pointing along the tetragonal c axis [001] and that pointing in the ab plane [110]. The [001] orientation of the M spin was found to be favorable in all cases except NiF_2 for which the [110] orientation was favored in good agreement with experimental findings.[16] In conformity with the d^5 configuration of Mn, the orbital moment at Mn is found to be tiny, less than $10^{-3}\mu_B$. The partially filled t_{2g} shell of the d^6 and d^7 configurations of Fe and Co gives rise to finite orbital moments though partially quenched due to the lifting of degeneracies within the t_{2g} manifold with values of $0.09\mu_B$ and $0.17\mu_B$, respectively. The orbital moment for Co is appreciably high as has been pointed out in experimental study.[4] Interestingly, we find the orbital moment for Ni to be also rather high, having a value of $0.19\mu_B$. This is unexpected since for Ni^{2+} with a filled t_{2g} shell and a half-filled e_g shell, the orbital moment would be quenched. This hints once again at the finite and appreciable hybridization of F p states as has been concluded in the study of Ref. 9. In the literature, the finite p-orbital mixing has been pointed out as a means of generating an appreciable SOC effect.[18]

V. MAGNETOELASTIC EFFECT

In the next step, to explore the magnetoelastic effect theoretically, we carried out structural optimization considering the ground-state magnetic configurations, i.e., A-AFM and a different magnetic configuration. Ideally, the other magnetic configuration should be the paramagnetic (PM) configuration. However, there is no simple prescription to simulate a PM phase in a DFT calculation. We, therefore, consider two different cases. In the first case, the structural changes upon changing the magnetic ordering from FM to A-AFM (cf. Theory I in Fig. 3) were calculated. In the second case, we assumed the PM phase to be mimicked by an average of different possible collinear spin configurations within a supercell of size $2 \times 2 \times 2$, which is eight times the unit cell and contains 16 M atoms in the unit cell. While in principle 2^{16} collinear spin arrangements are possible, among these only six different spin arrangements were chosen which are energetically nondegenerate and compatible with

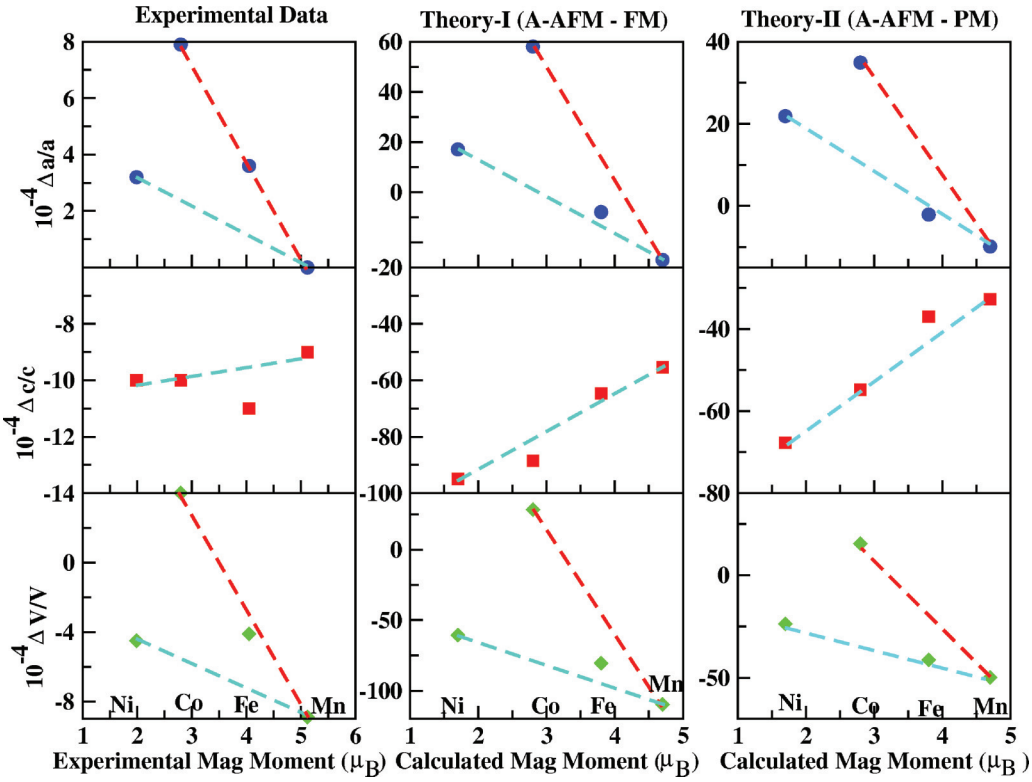

FIG. 3. (Color online) The relative changes in cell parameters upon a change in magnetic ordering for MF_2 (M = Mn, Fe, Co, and Ni). The leftmost panels show the experimental results (extracted out of data points presented in Refs. 3 and 4 while the middle and rightmost panels show the theoretical results (see text for details). Two straight lines have been plotted in the top and bottom panels in order to indicate the nonmonotonic behavior of the changes as a function of magnetic moment.

the symmetry of the unit cell. The calculations of structural changes were carried out for all of these six different spin configurations, and the average is considered to represent the PM state (Theory II in Fig. 3). The results are summarized in Fig. 3, together with experimental results, extracted out of data presented in Refs. 3 and 4. We find that while $\Delta c/c$ shows more or less monotonic behavior within the series MF_2 (M = Mn, Fe, Co, Ni), (with magnetic moments 5, 4, 3, and 2μ_B/f.u., respectively), the variation in a lattice parameter ($\Delta a/a$) is highly nonmonotonic. The nonmonotonic behavior of $\Delta a/a$ results in the nonmonotonic variation also in volume $\Delta V/V$, which is given by $2(\Delta a/a) + (\Delta c/c)$ for a crystal of tetragonal symmetry. This general trend obtained in theoretical calculations is in very good agreement with experimental measurements. We find $\Delta V/V$ to be relatively large and negative for MnF_2, those for FeF_2 and NiF_2 to be both negative, and that for CoF_2 to be small and positive in conformity with experimental findings. Considering the quantitative values, theoretical estimates for the first approach (Theory I) are found to be about a factor of ten larger, compared to experimental estimates. Using the supercell approach for defining the PM state (Theory II), the theoretical estimates are found to be smaller compared to Theory I but still a factor of five to six times larger, compared to experimental estimates. Nevertheless, the reduction of values between Theory II and Theory I indicates that mimicking the PM state correctly would presumably make the qualitative comparison between theory and experiment even better. The results presented in Fig. 3 have been obtained with the choice of the GGA exchange correlation. We find that the introduction of the missing correlation effect beyond the GGA, in the form of GGA+U calculations,[19] reduces the quantitative estimates even further. However, in the absence of a good prescription on the knowledge of variation of U across the Mn-Fe-Co-Ni series, we have adhered to the results obtained within the GGA calculations. One needs to note that such effects are very tiny effects (less than 0.1%), and therefore, it is a challenge both experimentally and theoretically to capture them properly. Keeping that in mind, the overall agreement is surprisingly good.

VI. ORIGIN OF NONMONOTONIC MAGNETOELASTIC BEHAVIOR

In order to probe the origin of the observed nonmonotonic magnetoelastic behavior among the studied series, we plot in Fig. 4 the change in various structural elements upon a change in magnetic ordering. The structural elements considered are (i) α_1, the AFM corner-shared M-F-M bond angle; (ii) α_2, the FM edge-shared M-F-M bond angle; (iii) d_1, the short M-F bond forming one edge of the AFM corner-shared interactions; and (iv) d_2, the long M-F bond forming the other edge of the AFM corner-shared interaction (cf. the marking in Fig. 1 for the visual representations) as well as M-F bonds of the edge-shared M-M interactions. Note that α_2 connects two M ions situated along the c axis and that the variation in α_2 essentially controls the variation in c together with that in d_2. α_1 connects two M ions situated halfway through the body-diagonal vector, and the variation effects the a, b, and c parameters equally. Among the d_1 and d_2 bonds, the d_1 bond lies strictly in the ab plane while the d_2 bond lies mostly

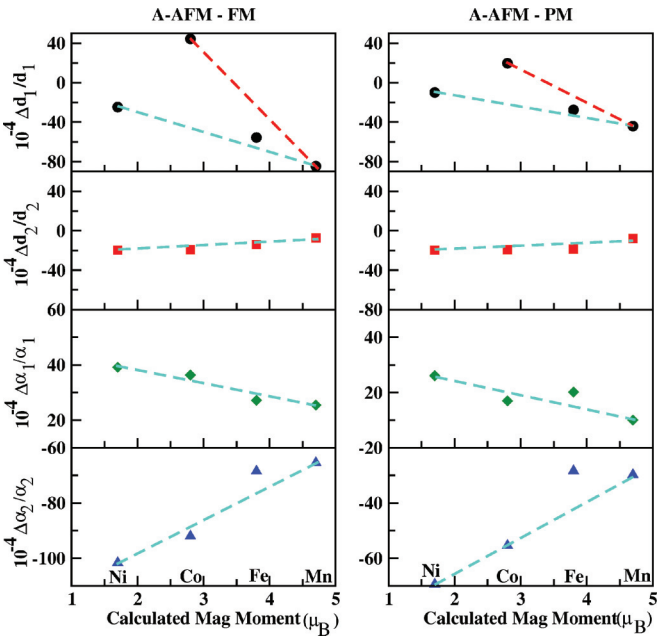

FIG. 4. (Color online) Calculated changes in structural parameters d_1, d_2, α_1, and α_2 in MF_2 upon a change in magnetic ordering. Two straight lines have been plotted in the top panels in order to indicate the nonmonotonic behavior of the changes as a function of magnetic moment.

along the c axis with a relatively smaller component in the ab plane. Focusing on the trend of variations of d_1, d_2, α_1, and α_2 as presented in Fig. 4, we find that while the variation of the change of d_2 and α_1 (especially d_2) across the series is mild and monotonic, that of α_2 is rather strong and monotonic, and that of d_1 is strong and highly nonmonotonic. It is rather interesting to note that the variation of the changes of α_2 and d_1 almost follows the nature of the variation of the change of "c" and "a" across the series as presented in Fig. 3. While the exact value of $\Delta a/a$ is determined by the variation of both $\Delta\alpha_1/\alpha_1$ and $\Delta d_1/d_1$ (the variation of $\Delta d_2/d_2$ being small), the nonmonotonic behavior of $(\Delta a/a)$ has its origin in the variation in $\Delta d_1/d_1$.

VII. EXCHANGE INTERACTIONS AND PHONONS

The magnetostriction or exchange striction is driven by the spin Hamiltonian $\sum_{ij} J\vec{S}_i\vec{S}_j$. The superexchange coupling J depends on (a) the $\angle M$-F-M, which is α_1 considering the nearest-neighbor AFM interaction in the present case as $\cos^2\alpha_1$ and (b) $t_{pd}^4/(\Delta + U)$, with t_{pd} being the hopping integral connecting the F p and M d levels, Δ being the energy-level separation between F p and M d levels, and U being the on-site Coulomb repulsion. t_{pd} depends on the M-F bond lengths (d_1, d_2). We extracted AFM nearest neighbor (NN) interaction, $J(J_1)$ from total energies of the AFM and FM configurations, calculated within the GGA+U with choice of $U = 3$ eV and $J_H = 0.9$ eV and mapping onto a Heisenberg model. The exchange interaction has been also obtained from neutron inelastic scattering (cf. Table IV in Ref. 11).[17] The theoretically obtained values of J_1 together with experimental estimates are shown in the top panel of Fig. 5. The chosen

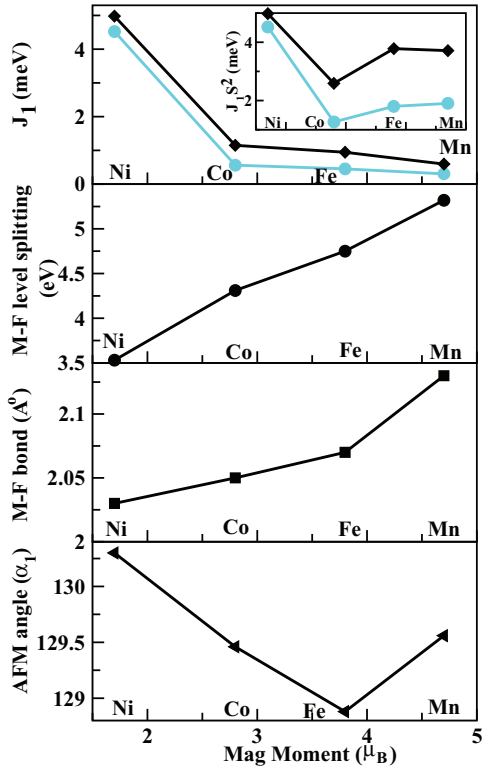

FIG. 5. (Color online) The top panel show the variation of the magnitude of the nearest-neighbor magnetic interaction J_1 plotted as a function of the magnetic moment, which increases progressively from NiF_2 to CoF_2 to FeF_2 to MnF_2. The inset shows the same for the quantity J_1S^2. The data points marked in cyan (light gray) are from experimental measurements (Ref. 17) while the points marked in black are theoretical estimates. The other three panels show the variation of the values of M-F level splitting, M-F bond length, and M-F-M bond angle across the series.

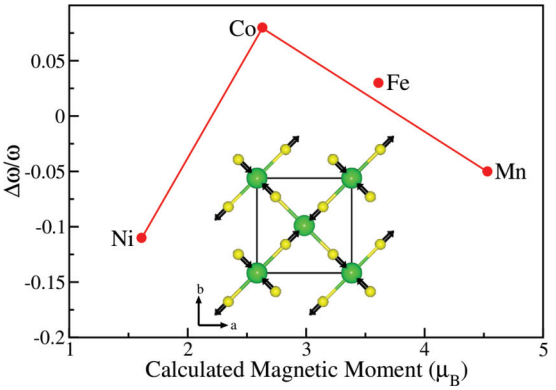

FIG. 6. (Color online) The relative change in phonon frequency, associated with the stretching of a short M-F bond length upon the change in magnetic ordering from FM to AFM for MF_2 compounds for M = Mn, Fe, Co, and Ni. The inset shows the atomic displacements associated with this phonon mode.

values of U and J_H provide good agreement between the calculated and measured values of J_1. We find the J_1 value for the NiF_2 compound is substantially larger compared to the rest in the series, which shows a gradual but small increase in values from MnF_2 to FeF_2 to CoF_2. This results in the highly nonmonotonic behavior of J_1S^2 as shown in the inset.

The other three panels of Fig. 5 show the variation in values of Δ, $\langle d \rangle$ (the average of d_1, d_2), and α_1 across the series. The relatively small Δ, together with small $\langle d \rangle$, which increases the t_{pd} value and relatively larger α_1, makes $J_1^{\text{Ni-Ni}}$ about a factor of five times larger compared to that of $J_1^{\text{Co-Co}}$, overcompensating the difference of S^2 between Ni^{2+} and Co^{2+}. J_1S^2 is, therefore, highly nonmonotonic across the series. The change in the J_1 value in two magnetic configurations ΔJ_1 can arise from the change in α_1 and $\Delta\alpha_1$ as well as from the change in $\langle d \rangle$, more appropriately in d_1, the change in d_2 being small. While commonly the magnetostriction giving rise to spin-phonon coupling is associated with the change of the superexchange angle upon the change in magnetic ordering,[20] we find that in the present case, the metal-anion distance, which dictates the strength of the virtual hopping t_{pd}, also adds on to the exchange-striction effect, especially in understanding the nonmonotonic behavior of exchange striction across the series. In order to further probe this issue, we calculate the normal-mode frequencies, which are of the symmetries A_{1g}, B_{1g}, A_{2g}, B_{2g}, E_g, B_{1u}, A_{2u}, and E_u for the FM and AFM spin configurations. We calculate the phonon frequencies of the structure optimized with the AFM spin configuration. Among the normal modes, the mode A_{1g} is associated with the stretching of the M-F short bond d_1 (cf. the inset in Fig. 6). We find that while for MnF_2 and NiF_2, the phonon frequency associated with the A_{1g} mode softens upon moving from the FM to AFM spin alignment, for CoF_2 and FeF_2 (for FeF_2 the change is small) it is the opposite, and the phonon frequency hardens in moving from the FM to AFM alignment as shown in Fig. 6. This presumably hints towards the differential behavior of a Jahn-Teller (JT) nature of the Fe^{2+} and Co^{2+} ions compared to the non-Jahn-Teller nature of the Mn^{2+} and Ni^{2+} ions. We note that Fe^{2+} in its d^6 ($d^5 + d^1$) configuration has one JT-active electron while Co^{2+} in its d^7 ($d^5 + d^2$) configuration has two JT-active electrons. This is expected to make the JT-influenced changes associated with the Co compound stronger than those in the Fe compound.

VIII. CONCLUSION

In conclusion, using first-principles DFT calculations we have explored the origin of nonmonotonic magnetoelastic effects across the 3d metal difluoride series MF_2 with M = Mn, Fe, Co, and Ni. Our first-principles calculations could successfully reproduce the magnetoelastic-effect-induced nonmonotonic changes in cell parameters for the series as observed experimentally.[3,4] Such an agreement is impressive as the effects are very small. We calculated magnetic exchange interactions as well as investigated magnetic anisotropy effects. Our study indicated the important role of M-F covalency, which has been also discussed in the literature.[9] The first-principles investigations showed that the nonmonotonic nature of exchange-striction-driven changes in the lattice across the MF_2 series originate essentially from the nonmonotonic behavior of the bond-stretching phonon mode associated with the short M-F bond. While normally attention is paid to the changes in the

metal- anion-metal superexchange angle, we find that it is the change in the metal-anion bond that plays the vital role in explaining the nonmonotonic behavior of the magnetoelastic effect across the MF_2 series with M = Mn, Fe, Co, Ni.

ACKNOWLEDGMENT

Work at Cornell by H.D. was supported by the DOE-BES under Award No. DE-SC0005032.

[1]P. J. Edwardson, L. L. Boyer, R. L. Newman, D. H. Fox, J. R. Hardy, J. W. Flocken, R. A. Guenther, and W. Mei, Phys. Rev. B **39**, 9738 (1989); C. G. Duan, W. N. Mei, J. Liu, W. G. Yin, J. R. Hardy, R. W. Smith, M. J. Mehl, and L. L. Boyer, *ibid*. **69**, 033102 (2004).

[2]G. Nenert and T. T. M. Palstra, J. Phys.: Condens. Matter **19**, 406213 (2007).

[3]T. Chatterji, G. N. Iles, B. Ouladdiaf, and T. C. Hansen, J. Phys.: Condens. Matter **22**, 316001 (2010).

[4]T. Chatterji, B. Ouladdiaf, and T. C. Hansen, J. Phys.: Condens. Matter **22**, 096001 (2010).

[5]C. Billy and H. M. Haendler, J. Am. Chem. Soc. **79**, 1049 (1957).

[6]T. Chatterji and T. C. Hansen, J. Phys.: Condens. Matter **23**, 276007 (2011).

[7]J. W. Cable, M. K. Wilkinson, and E. O. Wollan, Phys. Rev. **118**, 950 (1960).

[8]R. Schleck, Y. Nahas, R. P. S. M. Lobo, J. Varignon, M. B. Lepetit, C. S. Nelson, and R. L. Moreira, Phys. Rev. B **82**, 054412 (2010).

[9]P. J. Brown, B. N. Figgis, and P. A. Reynolds, J. Phys.: Condens. Matter **2**, 5297 (1990); **2**, 5309 (1990).

[10]G. Kresse and J. Hafner, Phys. Rev. B **47**, R558 (1993); G. Kresse and J. Furthmuller, *ibid*. **54**, 11169 (1996).

[11]O. K. Andersen and O. Jepsen, Phys. Rev. B **12**, 3060 (1975).

[12]O. K. Andersen and T. Saha-Dasgupta, Phys. Rev. B **62**, R16219 (2000).

[13]O. K. Andersen and O. Jepsen, Phys. Rev. Lett. **53**, 2571 (1984).

[14]P. Blaha, K. Schwartz, G. K. H. Madsen, D. Kvasnicka, and J. Luitz, in *WIEN2K, An Augmented Plane Wave + Local Orbitals Program for Calculating Crystal Properties*, edited by K. Schwarz (Technische Universitatâ Wien, Vienna, 2001).

[15]J. P. Perdew, K. Burke, and M. Ernzerhof, Phys. Rev. Lett. **77**, 3865 (1996).

[16]A. Palmes and W. Jauch, Solid State Commun. **77**, 95 (1991).

[17]M. T. Hutchings, M. F. Thorpe, R. J. Birgeneau, P. A. Fleury, and H. J. Guggenheim, Phys. Rev. B **2**, 1362 (1970).

[18]C. Jia, S. Onoda, N. Nagaosa, and J. H. Han, Phys. Rev. B **76**, 144424 (2007).

[19]V. I. Anisimov, I. V. Solovyev, M. A. Korotin, M. T. Czyzyk, and G. A. Sawatzky, Phys. Rev. B **48**, 16929 (1993).

[20]H. Das, U. V. Waghmare, T. Saha-Dasgupta, and D. D. Sarma, Phys. Rev. Lett. **100**, 186402 (2008).